THE JOURNAL OF PHYSICAL CHEMISTRY B

Article

pubs.acs.org/JPCB

Relaxation and Dissociation Following Photoexcitation of the $(\mu\text{-}N_2)[Mo(N[t\text{-}Bu]Ar)_3]_2$ Dinitrogen Cleavage Intermediate

Adam S. Huss,[†] John J. Curley,[‡] Christopher C. Cummins,[‡] and David A. Blank*[,†]

[†]Department of Chemistry, University of Minnesota, 207 Pleasant Street SE, Minneapolis, Minnesota 55455, United States

[‡]Department of Chemistry, Massachusetts Institute of Technology, 77 Massachusetts Avenue, Cambridge, Massachusetts 02139, United States

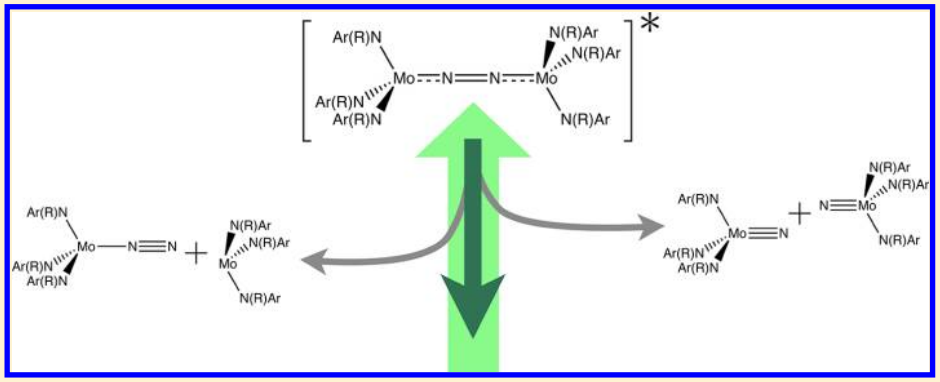

ABSTRACT: Frequency resolved pump−probe spectroscopy was performed on isolated $(\mu\text{-}N_2)[Mo(N[t\text{-}Bu]Ar)_3]_2$ (Ar = 3,5-$C_6H_3Me_2$), an intermediate formed in the reaction of $Mo(N[t\text{-}Bu]Ar)_3$ to bind and cleave dinitrogen. Evidence is presented for 300 fs internal conversion followed by subpicosecond vibrational cooling on the ground electronic state in competition with bond dissociation. Fast cooling following photoexcitation leads to a relatively low overall dissociation yield of 5%, in quantitative agreement with previous work [Curley, J. J.; Cooke, T. R.; Reece, S. Y.; Mueller, P.; Cummins, C. C. *J. Am. Chem. Soc.* **2008**, *130*, 9394]. Coupling of vibrational modes to the excitation and internal conversion results in a nonthermal distribution of energy following conversion, and this provides sufficient bias to allow the nitrogen cleavage reaction to compete with breaking of the Mo−NN bond despite a higher energetic barrier on the ground state.

INTRODUCTION

The chemical activation of molecular nitrogen is a topic that has received considerable attention. Interest is driven by both the broad potential application of molecular nitrogen as the starting point for incorporation of nitrogen-containing functional groups, and more focused goals such as the development of less demanding alternatives to the energetically intensive industrial production of ammonia.[1−5] One approach to this problem has focused on thermochemistry, with many recent studies in pursuit of reactive metal nitrides via thermally accessible cleavage of bimetallic μ-N_2 complexes.[6−14] By comparison, the use of energy in the form of light to assist in the activation of molecular nitrogen has received less attention. Reiher et al. computationally investigated $\pi^* \leftarrow \pi$ excitation of bimetallic μ-N_2 complexes to activate directed reduction of the nitrogen.[15] Their work investigated dissociation in an excited σ^* state and suggested a key role for bending of the core MoNNMo structure. Experimentally, there have been three reports of photolytic nitrogen cleavage products from such complexes. Floriani and co-workers concluded that cleavage of the nitrogen bond was the initial step in the photochemical reaction of thermally stable $(\mu\text{-}N_2)[Mo(Mes)_3]_2$ (Mes = 2,4,6-$Me_3C_6H_2$) based on conversion to $(Mes)_3Mo{-}N{-}Mo(Mes)_3$ under UV illumination.[13] Using ultraviolet excitation, Kunkely and Volger recently demonstrated dissociation of the nitrogen bond in a μ-N_2 diosmium cation.[16] In the longest wavelength activation reported, Curley et al. have observed that excitation of the strong visible absorption band in the isolated dinitrogen cleavage intermediate $(\mu\text{-}N_2)[Mo(N[t\text{-}Bu]Ar)_3]_2$ leads to breaking of both N≡N and Mo−NN bonds with roughly equal branching.[17,18]

The three-coordinate molybdenum(III) complex $Mo(N[t\text{-}Bu]Ar)_3$ reacts readily at mild temperatures and pressures (−35 to 30 °C, 1 atm) to cleave dinitrogen via the $(\mu\text{-}N_2)[Mo(N[t\text{-}Bu]Ar)_3]_2$ intermediate.[10,11,19] The complete reaction path, starting with N_2 and $Mo(N[t\text{-}Bu]Ar)_3$, is illustrated in Scheme 1. Recently, the $(\mu\text{-}N_2)[Mo(N[t\text{-}Bu]Ar)_3]_2$ intermediate was isolated and characterized via X-ray crystallography, and its electronic structure was studied using density functional theory.[17] Investigation of the compound's intense visible absorption band centered at 2.39 eV led to the discovery of a photochemical reaction that cleaves the metal nitrogen bond,

Received: October 12, 2012
Revised: December 18, 2012
Published: December 18, 2012

Scheme 1. Reproduced from Laplaza *et al.*[11]

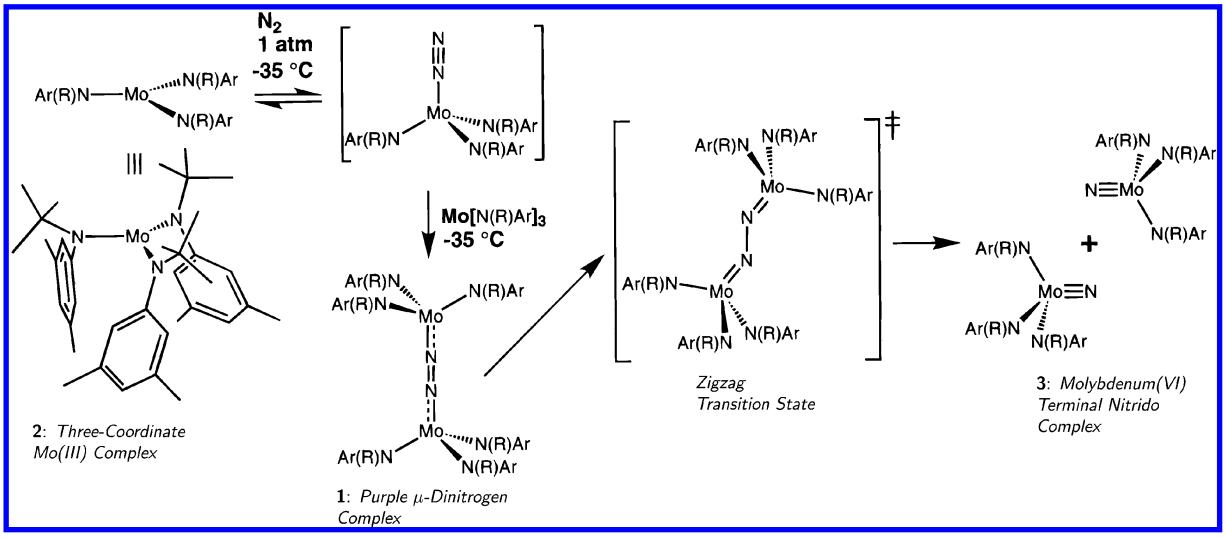

with subsequent extrusion of N_2 and reformation of the starting complex. This reaction was determined to compete with photochemical N≡N cleavage based on bulk photolysis at −78 °C that gives an approximate 1:1 mixture of N≡Mo(N[t-Bu]Ar)$_3$ and Mo(N[t-Bu]Ar)$_3$ with a primary quantum yield of 0.05. Initial transient absorption spectroscopy has shown that the photoreaction is complete in less than 10 ns, the time resolution of the experiment.

Compared to thermal pathways, photochemical pathways aimed at N_2 fixation are much less well-known and could tie into energy-saving (i.e., photochemical) nitrogen fixation schemes. The photolysis reaction offers the potential of storing reduced N_2 in the form of (μ-N_2)[Mo(N[t-Bu]Ar)$_3$]$_2$ with convenient, relatively low energy, targeted activation. To evaluate such potential, a better understanding of the photoexcitation dynamics, and the competition between N_2 extrusion via metal nitrogen bond cleavage and N≡N bond cleavage, is needed. In this work, the photolysis of (μ-N_2)[Mo(N[t-Bu]Ar)$_3$]$_2$ is studied with 60 fs time resolution. The observed dynamics are dominated by very rapid (sub-ps) internal conversion followed by vibrational cooling in the ground electronic state. However, incomplete recovery of the initial ground state bleach indicates the loss of ∼5% of the initially excited reactants. By placing the early time dynamics within the context of prior bulk photolysis experiments and computational results, a more complete and detailed picture of this photoinitiated reaction emerges.

EXPERIMENTAL SECTION

Preparation of (μ-N_2)[Mo(N[t-Bu]Ar)$_3$]$_2$, Figure 1 inset, has been reported elsewhere.[10,11,17,19,20] Approximately 0.07 mM diethyl ether solutions (ε = 41 000 M^{-1} cm^{-1} at 2.28 eV) of the sample were prepared in a glovebox and transferred to a sealed Schlenk flask that served as a sample reservoir. Due to the thermal and oxygen sensitivity of the compound, the reservoir was kept under high purity nitrogen using a mineral oil bubbler, and the temperature was kept at approximately −78 °C using a dry ice/ethanol bath. Sample solution was drawn through a 1 mm path length quartz flow cell using a peristaltic pump. The cell area was enclosed and exterior flooded with dry nitrogen in order to prevent condensation during pump probe experiments.

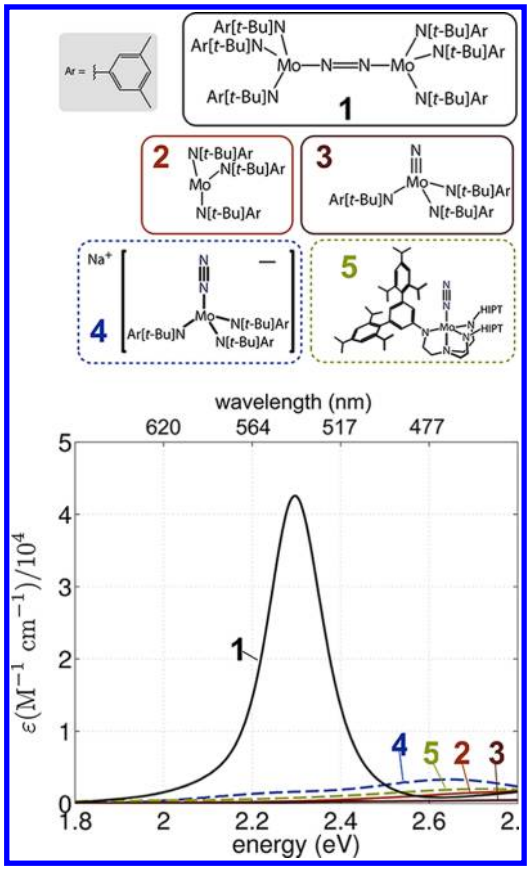

Figure 1. Absorption spectra and structures for the reactant, (μ-N_2)[Mo(N[t-Bu]Ar)$_3$]$_2$, **1**, potential photolysis products **2** and **3**, and surrogates for the absorption spectrum of potential photolysis products, **4** and **5**.

Absorption spectra taken before and after each pump probe run were indistinguishable, indicating a lack of sample degradation.

Absorption spectra were recorded using a Cary 14 spectrometer running the OLIS globalworks software suite. All other measurements were taken using a home-built, amplified ultrafast Ti:sapphire laser system, which has been described earlier.[21] Briefly, amplified, 400 μJ, 1.53 eV pulses were generated with fwhm (full width at half-maximum) of 70

dx.doi.org/10.1021/jp310122x | J. Phys. Chem. B 2013, 117, 1429−1436

fs at 1 kHz. The amplified fundamental was split, and the majority was used to to create excitation (pump) pulses at 2.32 eV, 60 fs fwhm, using a home built two stage noncollinear optical parametric amplifier (NOPA). The remaining 1.53 eV light was focused into a 3 mm thick piece of sapphire with a 15 cm lens to create a white light continuum probe (spanning 1.30−2.64 eV) that was subsequently collimated using a 2 cm focus parabola. The pump and probe were focused and crossed in the sample using a 5 cm focus parabola, with a resulting beam waist of ∼40 μm. Typical pump energies ranged from 50 to 75 nJ/pulse, and the measured signal was found to be linearly dependent on pump energy up to 100 nJ/pulse.

After traversing the sample, the probe continuum was collimated using a 5 cm lens and refocused into a Princeton Instruments 2150 monochromator after passing through a 1 mm cuvette containing an ethanol solution of 0.2 mM 1,1′-diethyl-4,4′ cyanine iodide (Sigma-Aldrich, used as received) which was used to filter out the residual 1.53 eV light from the laser fundamental. The probe was dispersed onto a 256 pixel silicon diode array (Hamamatsu). A National Instruments PCI-6132 A/D card was used to read the entire array after every laser shot at the laser repetition rate of 1 kHz. The pump beam was modulated at half the repetition rate using a chopper wheel, and the change in optical density, ΔOD, was recorded for every shot pair. Each spectrum was typically averaged for 90 000 laser shots. The relative polarization of the pump and probe was set to the magic angle (54.7°) to remove anisotropic dynamics. The instrument response was measured by crossing the probe continuum with the pump beam in an 80 μm thick type 1 BBO crystal (Super Optronics) cut for SFG in between 1.65 and 2.75 eV, and was found to be relatively independent of probe wavelength at 60 fs fwhm. Measurement of the cross phase modulation (XPM) in the neat solvent between the pump and a series of probe energies in the range 1.65−2.58 eV was used to determine the inherent chirp across the continuum probe.[22−24] The XPM determined time offsets were fit to a quadratic dispersion function, which was used to time correct the measured pump−probe spectra at each probe energy. Full frequency data was supplemented with pump−probe transients taken at individual probe wavelengths selected with a 10 nm fwhm interference filter and detected with a photodiode (Thorlabs DET-210) at the laser repetition rate.

CALCULATIONS

All DFT calculations were performed using the ADF2007 computer program.[25−27] Atomic coordinates for a theoretically optimized structure of (μ-N_2)[Mo(N[t-Bu]Ar)$_3$]$_2$ have been reported previously.[17] The input coordinates were obtained by an X-ray crystallographic study, and the geometry optimization was restricted to C_2 symmetry which was present in the crystallographic data. A time-dependent DFT calculation was performed upon the geometrically optimized structure of (μ-N_2)[Mo(N[t-Bu]Ar)$_3$]$_2$, using the BLYP functional which combines the exchange model proposed by Becke[28] with the correlation term proposed by Lee, Yang, and Parr (LYP).[29−31] All atoms were treated with basis sets that are double-ζ, or larger. Specifically, Mo was treated with the TZ2P basis set, and N was treated with DZP basis set.[32] Orbital contour plots were rendered using the DGRID computer package.[33] For complete details of these calculations see ref 18.

Vibrational frequencies were calculated for a simpler model complex that was constructed from the crystallographic coordinates of (μ-N_2)[Mo(N[t-Bu]Ar)$_3$]$_2$ by replacing the anilide ligands with hydrogen atoms using a N−H bond distance of 1.02 Å. The placement of the hydrogen atoms preserved the C−N−Mo−N dihedral angles that were present in the crystallographically determined structure. Numerical frequency calculations performed using these models indicated no negative frequencies, and geometry optimization was not performed. Numerical frequency calculations were performed using the OLYP functional which is a combination of the OPTX exchange correction presented by Handy and Cohen[34] and the LYP correlation model.[29−31]

RESULTS AND ANALYSIS

Absorption. Absorption spectra and structures for (μ-N_2)[Mo(N[t-Bu]Ar)$_3$]$_2$, Mo(N[t-Bu]Ar)$_3$, N≡Mo(N[t-Bu]-Ar)$_3$, and two surrogates for the absorption of N≡N···Mo(N-[t-Bu]Ar)$_3$, which has not been isolated, are shown in Figure 1. The absorption of (μ-N_2)[Mo(N[t-Bu]Ar)$_3$]$_2$ peaks at 2.3 eV with an extinction coefficient of 41 000 M^{-1} cm^{-1}. The products and surrogates all exhibit much weaker, broader, and higher energy absorption than (μ-N_2)[Mo(N[t-Bu]Ar)$_3$]$_2$.

Pump−Probe Measurements and Fitting. Pump−probe spectra following excitation at 2.32 eV are presented in Figure 2. Transients collected at individual probe energies are shown in Figure 3a. These transients were fitted as a series of first order transitions, eq 1.

$$a(t)\mathbf{A} \xrightarrow{\tau_1} b(t)\mathbf{B} \xrightarrow{\tau_2} c(t)\mathbf{C} \xrightarrow{\tau_3} \cdots \quad (1)$$

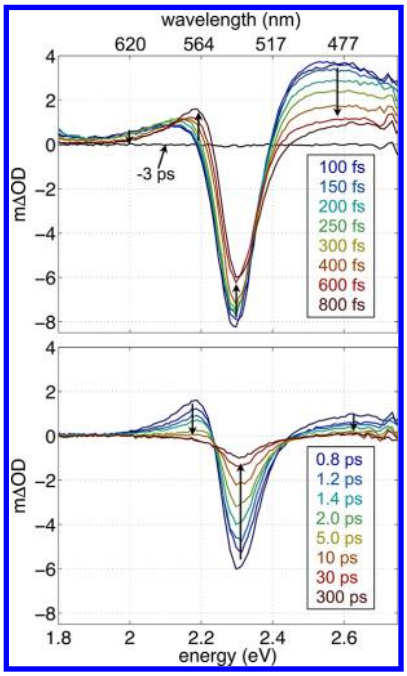

Figure 2. Pump−probe spectra for (μ-N_2)[Mo(N[t-Bu]Ar)$_3$]$_2$ at −78 °C in diethyl ether following excitation at 2.32 eV.

The bold capital letters (**A**, **B**, ...) represent the signal values and the τ_n values are the time constants for each transition. The lower case letters ($a(t)$, $b(t)$, ...) are the time dependent coefficients, which are constrained to a sum of 1 and are determined by solving the associated differential equations.[35] The initial condition is set with $a(0) = 1$ and $\mathbf{A} = 0$. The signal value as a function of time is given by eq 2.

dx.doi.org/10.1021/jp310122x | J. Phys. Chem. B 2013, 117, 1429−1436

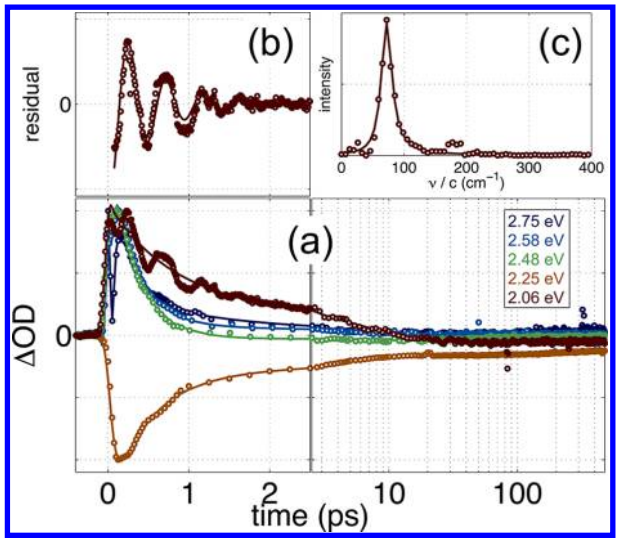

Figure 3. (a) Single color probe transients (probe energies indicated in the legend) taken following 2.32 eV excitation. For comparison, data are scaled to the same maximum value. For absolute ΔOD values at different probing energies see Figure 2. (b) The residual from the fit to the 2.06 eV probe data in panel a. (c) The modulus squared Fourier transform of the plot in panel b. Fit constants are given in Table 1. In all panels the circles are the raw data and solid lines represents fits to the data as described in the text.

$$S(t) = a(t)\mathbf{A} + b(t)\mathbf{B} + c(t)\mathbf{C} + \cdots \quad (2)$$

This functional form was chosen to characterize the time scales primarily based on the ability to accurately model the data with the minimum number of adjustable parameters. Equation 2 was convoluted over the instrument response, and the amplitudes and time constants were optimized to minimize the difference between the model and the data. The optimized fitting parameters are presented in Table 1, and the corresponding fits are compared to the data in Figure 3a. A minimum number of steps in eq 1 was used to produce a good fit. The minimum number of steps was determined by a lack of statistical improvement in the fit with the addition of a subsequent step.

Initial Excitation. In Figure 2 the transient spectrum appears within the instrument time resolution of 60 fs, τ_1 in Table 1. It is composed of a sharp negative feature peaked at 2.3 eV and a broad positive contribution that extends beyond the high energy range of the probe window. These contributions are illustrated in Figure 4a, where the spectrum

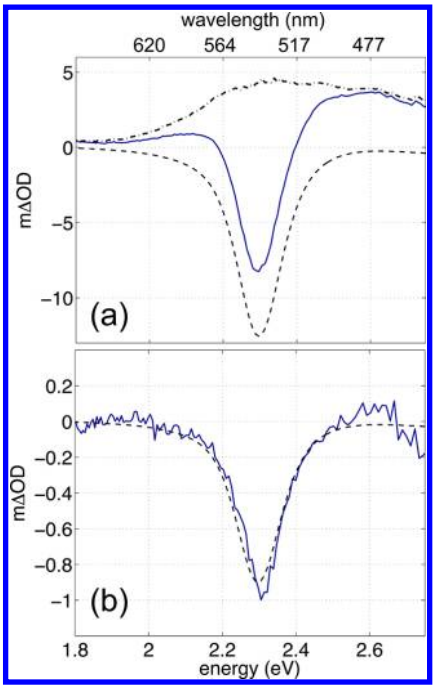

Figure 4. Solid line is the pump−probe spectrum at a probe delay of (a) 100 fs and (b) 300 ps. The dashed line is the inverted absorption spectrum representing the ground state hole. The dash−dot line in part a is the difference between the pump−probe spectrum and the ground state hole, representing the transient absorption at a probe delay of 100 fs.

at a time delay of 100 fs has been decomposed into the broad absorption from the excited state and the corresponding hole in the ground state absorption. Analysis of the DFT calculations suggests that the absorption at 2.3 eV primarily involves excitation from the triplet ground state of $(\mu\text{-}N_2)[Mo(N[t\text{-}Bu]Ar)_3]_2$ to the second excited triplet state. The orbitals involved are shown in Figure 5. This $e_g^4e_u^2$ to $e_g^3e_u^3$ type transition is localized on the MoNNMo core of the molecule and involves a shift in electron density from an orbital with Mo−N bonding and NN antibonding character to one with Mo−N antibonding and NN bonding character.

Residual Bleach and Dissociation Yield. At long delay times the spectrum that remains is primarily composed of a residual ground state hole, as shown in Figure 4b. By 50 ps the spectrum is nearly identical to that reported by Curley et al. after excitation with a 10 ns laser pulse.[17] There is some indication of broad residual absorption around 2.6 eV, which

Table 1. Fitting Parameters for the Single Color Probe Transients in Figure 3a[a]

	probe energy (eV)				
fitting param	2.75	2.58	2.48	2.25	2.06
τ_1 (fs)	<60	<60	<60	<60	<60
τ_2 (fs)	238 ± 30	299 ± 11	329 ± 6	461 ± 18	808 ± 94
τ_3 (ps)	1.61 ± 0.25	4.02 ± 1.21		3.52 ± 0.30	6.81 ± 1.43
τ_4 (ps)				340 ± 120	
A (mΔOD)	0	0	0	0	0
B (mΔOD)	4.14 ± 0.23	5.71 ± 0.07	5.09 ± 0.07	−6.12 ± 0.05	1.07 ± 0.03
C (mΔOD)	0.83 ± 0.13	0.29 ± 0.06	0.10 ± 0.01	−1.59 ± 0.07	0.23 ± 0.05
D (mΔOD)	0.05 ± 0.01	0.03 ± 0.007		−0.77 ± 0.01	−0.05 ± 0.01
E (mΔOD)				−0.52 ± 0.05	

[a]Errors are reported as the 68.2% confidence interval in the nonlinear fitting when all variables are simultaneously optimized with **A** held fixed at 0.

dx.doi.org/10.1021/jp310122x | J. Phys. Chem. B 2013, 117, 1429−1436

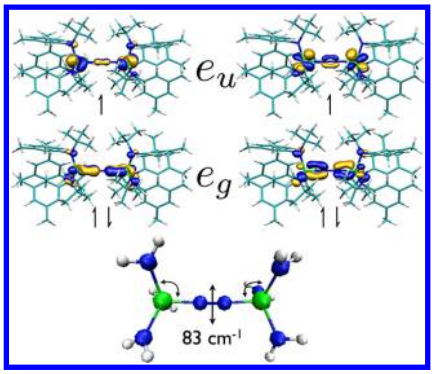

Figure 5. Top: Molecular orbitals involved in the intense absorption at 2.29 eV for $(\mu\text{-}N_2)[Mo(N[t\text{-}Bu]Ar)_3]_2$. Details of the transition and the calculation are described in the text. Ground state occupancy is shown. Bottom: Calculated 83 cm^{-1} MoNNMo core cis bending mode for model system $(\mu\text{-}N_2)[Mo(N[t\text{-}Bu]Ar)_3]_2$.

corresponds to the region where the dissociation products absorb, see Figure 1. However, given the quality of the data, the limited differentiation between the spectral shapes of potential bond cleavage products, and the relatively small absorption cross sections for the products compared with $(\mu\text{-}N_2)[Mo(N[t\text{-}Bu]Ar)_3]_2$, we are not able to positively identify dissociation products or quantify product ratios.

Incomplete recovery of the absorption hole at long delay time provides an upper limit for the overall dissociation yield. This requires calculating the fraction of the initial bleach that remains at long delay times. The absorption hole is probed at 2.25 eV, see Table 1. The initial amplitude is **B** = −6.12 (mΔOD). This signal includes both the negative hole and the positive excited state absorption. The ratio of the initial bleach to the measured signal at 2.25 eV is 1.54, see Figure 4a. Accounting for the excited state absorption, the initial value for the bleach is −9.42. The bleach amplitude at large delay is **E** = −0.52, and this has no contribution from excited state absorption as discussed below. Therefore, the remaining bleach of the $(\mu\text{-}N_2)[Mo(N[t\text{-}Bu]Ar)_3]_2$ starting material on the 500 ps time scale of the experiments here is 5.5% of the initial value. This is in excellent agreement with the overall dissociation quantum yield of 0.05 determined for bulk photolysis.[17]

Excited State Decay via Rapid Internal Conversion. At probe energies >2.5 eV the pump−probe spectra are composed primarily of transient absorption in the excited state and are dominated by a 300 fs decay with a minor component on a ∼2 ps time scale, Figures 2 and 3, and Table 1. The rapid decay is accompanied by the appearance of a new absorption around 2.2 eV. After 1 ps very little excited state absorption remains and the transient spectra take on a differential shape in the region of the $(\mu\text{-}N_2)[Mo(N[t\text{-}Bu]Ar)_3]_2$ absorption band. This shape is indicative of a vibrationally hot ground state. There is enhanced absorption on the low energy side of the absorption band by the hot ground state $(\mu\text{-}N_2)[Mo(N[t\text{-}Bu]Ar)_3]_2$ molecules, and this is summed with their associated ground state bleach in the cold absorption spectrum to give the overall differential appearance.

To better isolate the ground state dynamics we can subtract the excited state contribution from the transient spectra in Figure 2. The excited state contribution includes both the excited state absorption and the ground state hole associated with the excited state molecules. The total excited state spectrum is modeled as the initial pump−probe spectrum at a time delay of 100 fs, Figure 4a. When subtracting this from the raw data at all time delays we first scale the excited state spectrum to match the raw data in the probe window 2.60−2.64 eV, which assumes that the spectrum in this range is dominated by the excited state absorption. This energy region is at the minimum in the ground state hole (i.e., a minimum in the ground state absorption spectrum), and there will be very little contribution from any of the potential dissociation products due to the combination of small relative absorption cross sections and the small dissociation yields outlined above. The results are presented in Figure 6.

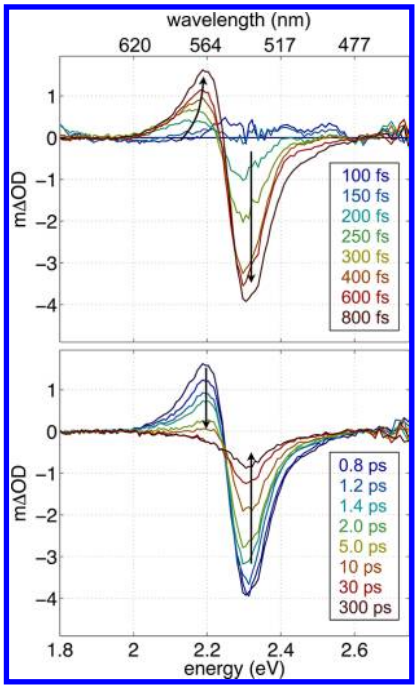

Figure 6. Transient spectra at the indicated probe delays following subtraction of the excited state absorption and its associated ground state hole, as described in the text.

The residual pump−probe spectra in Figure 6 rapidly build in from zero with the differential shape of an energetic ground state and a clear spectral shift of the positive hot absorption around 2.19 eV to higher energy in the first 800 fs. This spectral shift and the sub-ps rise of the hot ground state are well correlated with the 300 fs decay in the excited state absorption. The hot ground state spectrum is clearly evident in Figure 6 by 200 fs. In the absence of evidence for the participation of any other states, and given the direct evidence for very rapid transfer to the ground state, we conclude that the initial photoexcited state is primarily deactivated via internal conversion (IC) to the ground state in 300 fs. This is subsequently followed by competition between dissociation and vibrational cooling.

Vibrational Cooling. The rate of vibrational cooling following IC is probed via decay of the hot absorption on the low energy side of the $(\mu\text{-}N_2)[Mo(N[t\text{-}Bu]Ar)_3]_2$ absorption band at 2.06 eV. The data show the majority (∼80%) of the cooling taking place with a time constant of 800 fs followed by a subsequent decay with a time constant of 7 ps, see Table 1. Although initially there is some contribution to the absorption from the excited state at 2.06 eV, see Figure 4, this additional contribution is small and decays rapidly, in 300 fs.

dx.doi.org/10.1021/jp310122x | J. Phys. Chem. B 2013, 117, 1429−1436

Figure 7 shows the time evolution of the hot ground state absorption after subtraction of the excited state absorption

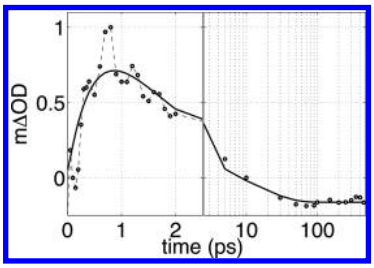

Figure 7. Average ΔOD in the range 2.00−2.23 eV from the data in Figure 6. The solid line is the fit as described in the text.

averaged over the 2.00−2.23 eV probe range in Figure 6. After subtraction of the contributions from the excited state, both the initial rise and the subsequent decay of the hot ground state absorption reflect vibrational cooling. A fit to these data using eq 1 finds that both the rise and the primary decay take place on a time scale of 800 ± 300 fs, supporting the dominant rapid cooling rate indicated in the higher signal-to-noise raw data at 2.06 eV in Figure 3. Although the subtracted data are sparse at time delays beyond 2 ps, the fit in Figure 6 is improved by including a small, poorly quantified, additional decay with a time constant of 17 ± 33 ps. Overall, vibrational cooling after internal conversion takes place very rapidly, with the majority of the relaxation complete in <1 ps.

Coherent Vibrational Beat. There is an underdamped oscillation in the pump−probe decay at 2.06 eV in Figure 3a. This is more clearly illustrated by the residual (raw data minus the fit in Table 1) in Figure 3b and the associated Fourier transform in Figure 3c. The residual was fitted with an exponentially damped cosine function, eq 3.

$$S(t) = \exp\left(-\frac{t}{\tau_{\text{damp}}}\right)\cos\left\{2\pi\left(\frac{t}{\tau_{\text{period}}}\right) - \phi\right\} \quad (3)$$

Nonlinear least-squares optimization resulted in a τ_{period} = 460 fs (73 cm^{-1}), τ_{damp} = 510 fs (10 cm^{-1}), and a phase shift of $\phi = 1.1\pi$. The fit is shown with the data in Figure 3b,c. The subperiod lifetime of the exited state, the phase of the beat, and the enhanced contrast on the low energy side of the absorption together strongly suggest that this is a vibration in the electronic ground state. The beats are clearly evident after subtraction of the excited state contribution to the pump−probe, as shown in Figure 7.

Energetically, the closest vibrations identified in the DFT calculations were two primarily ligand based modes at 69.5 cm^{-1} and 92.0 cm^{-1}, a trans bending mode of the MoNNMo core that included displacements in the ligands at 99.4 cm^{-1}, and a mode at 82.9 cm^{-1} that was a fairly well isolated cis bending mode of the core as illustrated in Figure 5. With the excitation at 2.3 eV isolated on the MoNNMo core, we favor assignment of the beat to the cis bending mode, with the possibility of some participation from the trans bending mode as well. Although both modes are predicted to be higher in energy than the observed 73 cm^{-1} mode, the calculated energies are expected to be overestimates due to truncation of the ligands in the DFT computation. Overall, the beat provides evidence of relatively strong coupling between nuclear displacement in the MoNNMo core and the electronic excitation. Coupling of this type is also supported by the prior observation of a strong resonance Raman band at 1630 cm^{-1} assigned to displacement in the N═N distance.[11,17]

DISCUSSION

The fact that the $(\mu\text{-}N_2)[Mo(N[t\text{-}Bu]Ar)_3]_2$ intermediate is kinetically stable and can be isolated at low temperature allows the opportunity to investigate the photochemistry of this important nitrogen cleavage intermediate. The initial bulk photolysis work by Curley et al. found that excitation in the intense absorption band at 2.3 eV not only leads to a modest yield for nitrogen cleavage (~2.5%), but simultaneously gives an equivalent yield of Mo−NN bond cleavage products.[17] They also determined that the dynamics take place in less than 10 ns, the time resolution of the experiment. Using much higher time resolution in the present study, we have found that the dynamics following excitation are dominated by a very rapid, 300 fs, return to the ground state and subsequent vibrational cooling. The overall dissociation yield is established in less than 500 ps. This remains an upper limit because the pump−probe spectra are dominated by vibrationally excited reactants and their associated cooling, which preclude a precise determination of reactant loss at early delay times. However, the transient spectrum is nearly indistinguishable from that reported by Curley et al. within 50 ps, indicating that dissociation takes place prior to complete vibrational cooling. The asymptotic value of reactant loss, determined after vibrational cooling is complete at 500 ps, is in quantitative agreement with the bulk photolysis yields.

One possible explanation for rapid excited state deactivation is a dissociative excited state that rapidly returns to the ground state via solvent-cage mediated geminate recombination. However, there is no evidence that the excited state is dissociative. Although the DFT calculations suggest a potential weakening of the Mo−NN bonds in the excited state, the excitation does not appear to have the σ^*-type character typically associated with impulsive bond cleavage. In systems that exhibit direct dissociation followed by geminate recombination, such as molybdenum complex dimers, the dissociation yields are much higher than the overall 5%, and 2.5% for an isolated bond cleavage channel, determined for $(\mu\text{-}N_2)[Mo(N[t\text{-}Bu]Ar)_3]_2$. The reported yields for direct dissociation of molybdenum complex dimers range from 26% to 73% depending on solvent and are independent of ligand size and mass.[36−39] Geminate recombination time scales in these cases are all reported around 5 ps, which is significantly slower than the sub-ps return to the ground state measured for $(\mu\text{-}N_2)[Mo(N[t\text{-}Bu]Ar)_3]_2$.

In addition to the comparatively low overall dissociation yields and faster conversion to the ground state, the possibility of an initial direct dissociation must also be evaluated together with the observation of nearly equal cleavage of the N═N and Mo−NN bonds.[17] In a scenario where excited state dissociation along Mo−NN precedes competition between recombination to a hot ground state and solvent cage escape to produce the Mo−NN cleavage products, producing an equivalent yield from dinitrogen cleavage would require preferential breaking of the N═N bond on the ground state. This seems unlikely due to the lower barrier to Mo−NN cleavage on the ground state (discussed below, see Figure 8) combined with the bias for initial vibrational energy deposition along the Mo−NN bond that would be produced by geminate recombination.

An alternative explanation for the rapid deactivation of the excited state is direct IC to the vibrationally excited ground

dx.doi.org/10.1021/jp310122x | J. Phys. Chem. B 2013, 117, 1429−1436

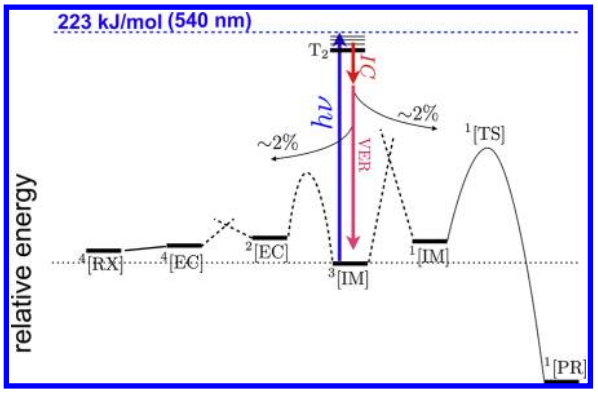

Figure 8. Illustration of the approximate energy landscape, adapted from Brookes et al.[40] RX: reactants, $Mo(N[t\text{-}Bu]Ar)_3$. EC: encounter complex, N N···$Mo(N[t\text{-}Bu]Ar)_3$. IM: intermediate, $(\mu\text{-}N_2)[Mo(N[t\text{-}Bu]Ar)_3]_2$. TS: transition state. PR: products, N≡$Mo(N[t\text{-}Bu]Ar)_3$. IC: internal conversion. VER: vibrational energy relaxation.

state. This is more consistent with the current evidence than competition with excited state dissociation. IC rates are enhanced by large coupling of the excitation to nuclear displacements. The DFT prediction indicates localization of the initial excitation around the MoNNMo core. Strong coupling to bending of the core is shown by the vibrational beat at 73 cm^{-1}, and the strong feature in the resonance Raman around 1600 cm^{-1} demonstrates coupling to the N═N distance.[11,17] The result is an initial step in the dynamics that involves IC to the ground state in 300 fs with some bias for vibrational energy deposition into modes that involve distortion of the MoNNMo core.

Once on the ground state, the dynamics become a competition between bond cleavage and vibrational energy relaxation, VER. Figure 8 presents an illustration of the energy landscape. The relative energies are approximated on the basis of the computational study by Brookes et al., including the barrier to dissociation of the singlet intermediate (IM) and the crossing between the triplet and singlet intermediate.[40] A low barrier between the doublet and quartet encounter complexes (EC) is based on the failure to observe N≡N···$Mo(N[t\text{-}Bu]Ar)_3$ following one electron oxidation of the anion, leading to the conclusion that there is very rapid conversion to the dissociative quartet and subsequent nitrogen extrusion.[17] Relatively low overall yield for dissociation reflects a failure to compete successfully with very rapid VER. The majority of the vibrational cooling takes place in about 1 ps.

With different barriers to N═N and Mo−NN cleavage, nearly equal yields[17] must reflect the nonstatistical distribution of vibrational energy that follows IC. Coupling between distortion of the MoNNMo core and the change in electronic state biases the limited dissociation in favor of the N═N cleavage channel. This is consistent with the required reorganization of the linear triplet intermediate to the *zigzag* singlet IM structure en route to singlet N≡$Mo(N[t\text{-}Bu]Ar)_3$ products.[11,41] The nonstatistical vibrational energy distribution may allow the higher barrier N═N cleavage channel to initially compete with Mo−NN bond breaking. However, the rate of VER is much faster than either dissociation branch, making recovery of the starting material the dominant channel following photoexcitation at 2.3 eV.

CONCLUSION

Photoexcitation of $(\mu\text{-}N_2)[Mo(N[t\text{-}Bu]Ar)_3]_2$ at 2.3 eV creates a very short-lived excited triplet state that undergoes internal conversion to the ground state in 300 fs. Rapid IC is facilitated by coupling of structural distortions in the MoNNMo core, and sub-ps vibrational cooling on the ground state inhibits effective competition from bond dissociation channels. This results in a small dissociation yield of around 5%. The previous observation of roughly equal amounts of N═N and Mo−NN bond cleavage, despite a higher barrier to N═N dissociation on the ground state, is rationalized in terms of the nonthermal vibrational energy distribution created by IC. Coupling of distortions in the MoNNMo core to IC assists in crossing to the singlet $(\mu\text{-}N_2)[Mo(N[t\text{-}Bu]Ar)_3]_2$ intermediate and provides some initial bias to the N═N dissociation path. Although the dissociation yield is small, enhancement in nitrogen cleavage over return to reactants as compared with thermal branching is an intriguing result. The photoexcitation dynamics indicate that yields following visible excitation would improve with inhibition of the VER rates, which might be possible via ligand modification and choice of surrounding media. Alternatively, access to dissociative excited states using shorter wavelength light would likely offer more dramatic enhancement in the dissociation yields.

AUTHOR INFORMATION

Corresponding Author

*E-mail: blank@umn.edu.

Notes

The authors declare no competing financial interest.

ACKNOWLEDGMENTS

This material is based upon work supported by the National Science Foundation under CHE-1111357 and CHE-719157. The authors would like to thank Andrei Tokmakoff for helpful discussions and suggesting this collaboration.

REFERENCES

(1) Chatt, J.; Dilworth, J. R.; Richards, R. L. *Chem. Rev.* **1978**, *78*, 589−625.
(2) Gambarotta, S. *J. Organomet. Chem.* **1995**, *500*, 117−126.
(3) Kozak, C. M.; Mountford, P. *Angew. Chem., Int. Ed.* **2004**, *43*, 1186−1189.
(4) MacKay, B. A.; Fryzuk, M. D. *Chem. Rev.* **2004**, *104*, 385−401.
(5) Tuczek, F.; Lehnert, N. *Angew. Chem., Int. Ed.* **1998**, *37*, 2336−2338.
(6) Caselli, A.; Solari, E.; Scopelliti, R.; Floriani, C.; Re, N.; Rizzoli, C.; Chiesi-Villa, A. *J. Am. Chem. Soc.* **2000**, *122*, 3652−3670.
(7) Clentsmith, G. K. B.; Bates, V. M. E.; Hitchcock, P. B.; Cloke, F. G. N. *J. Am. Chem. Soc.* **1999**, *121*, 10444−10445.
(8) Figueroa, J. S.; Piro, N. A.; Clough, C. R.; Cummins, C. C. *J. Am. Chem. Soc.* **2006**, *128*, 940−950.
(9) Kawaguchi, H.; Matsuo, T. *Angew. Chem.* **2002**, *114*, 2916−2918.
(10) Laplaza, C. E.; Cummins, C. C. *Science* **1995**, *268*, 861−863.
(11) Laplaza, C. E.; Johnson, M.; Peters, J. C.; Odom, A. L.; Kim, E.; Cummins, C. C.; George, G. N.; Pickering, I. J. *J. Am. Chem. Soc.* **1996**, *118*, 8623−8638.
(12) Mindiola, D. J.; Meyer, K.; Cherry, J. P. F.; Baker, T. A.; Cummins, C. C. *Organometallics* **2000**, *19*, 1622−1624.
(13) Solari, E.; Da Silva, C.; Iacono, B.; Hesschenbrouck, J.; Rizzoli, C.; Scopelliti, R.; Floriani, C. *Angew. Chem., Int. Ed.* **2001**, *40*, 3907−3909.
(14) Zanotti-Gerosa, A.; Solari, E.; Giannini, L.; Floriani, C.; Chiesi-Villa, A.; Rizzoli, C. *J. Am. Chem. Soc.* **1998**, *120*, 437−438.

(15) Reiher, M.; Kirchner, B.; Hutter, J.; Sellmann, D.; Hess, B. *Chem.—Eur. J.* **2004**, *10*, 4443−4453.
(16) Kunkely, H.; Vogler, A. *Angew. Chem., Int. Ed.* **2010**, *49*, 1591−1593.
(17) Curley, J. J.; Cook, T. R.; Reece, S. Y.; Mueller, P.; Cummins, C. C. *J. Am. Chem. Soc.* **2008**, *130*, 9394−9405.
(18) Curley, J. J. *Dinitrogen Fixation Chemistry of a Molybdenum Trisanilide System*. Ph.D. Thesis, Massachusetts Institute of Technology, http://hdl.handle.net/1721.1/49549, 2009.
(19) Laplaza, C. E.; Johnson, A. R.; Cummins, C. C. *J. Am. Chem. Soc.* **1996**, *118*, 709−710.
(20) Peters, J.; Cherry, J.; Thomas, J.; Baraldo, L.; Mindiola, D.; Davis, W.; Cummins, C. *J. Am. Chem. Soc.* **1999**, *121*, 10053−10067.
(21) Wells, N. P.; Boudouris, B. W.; Hillmyer, M. A.; Blank, D. A. *J. Phys. Chem. C* **2007**, *111*, 15404−15414.
(22) Dietzek, B.; Pascher, T.; Sundstrom, V.; Yartsev, A. *Laser Phys. Lett.* **2007**, *4*, 38−43.
(23) Healy, A. T.; Lipsky, S.; Blank, D. A. *J. Chem. Phys.* **2007**, *127*, 214508.
(24) Kovalenko, S.; Dobryakov, A.; Ruthmann, J.; Ernsting, N. *Phys. Rev. A* **1999**, *59*, 2369−2384.
(25) Baerends, E. J.; et al. *ADF2007.01*; SCM, 2007.
(26) Velde, G.; Bickelhaupt, F.; Baerends, E.; Guerra, C.; Gisbergen, S. V.; Snijders, J.; Ziegler, T. *J. Comput. Chem.* **2001**, *22*, 931−967.
(27) Guerra, C.; Snijders, J.; te Velde, G.; Baerends, E. *Theor. Chem. Acc.* **1998**, *99*, 391−403.
(28) Becke, A. D. *Phys. Rev. A* **1988**, *38*, 3098−3100.
(29) Johnson, B.; Gill, P. M. W.; Pople, J. A. *J. Chem. Phys.* **1993**, *98*, 5612−5626.
(30) Lee, C.; Yang, W.; Parr, R. *Phys. Rev. B* **1988**, *37*, 785−789.
(31) Russo, T. V.; Martin, R. L.; Hay, P. J. *J. Chem. Phys.* **1994**, *101*, 7729−7737.
(32) Chong, D. *Mol. Phys.* **2005**, *103*, 749−761.
(33) Kohout, M. *DGrid Progam 4.3 ed.*; 2008.
(34) Handy, N.; Cohen, A. *Mol. Phys.* **2001**, *99*, 403−412.
(35) Schmidtke, S.; Underwood, D. F.; Blank, D. A. *J. Phys. Chem. A* **2005**, *109*, 7033−7045.
(36) Oelkers, A. B.; Scatena, L. F.; Tyler, D. R. *J. Phys. Chem. A* **2007**, *111*, 5353−5360.
(37) Oelkers, A. B.; Schutte, E. J.; Tyler, D. R. *Photochem. Photobiol. Sci.* **2008**, *7*, 228−234.
(38) Oelkers, A. B.; Tyler, D. R. *Photochem. Photobiol. Sci.* **2008**, *7*, 1386−1390.
(39) Baiz, C. R.; McCanne, R.; Kubarych, K. J. *J. Am. Chem. Soc.* **2009**, *131*, 13590−13591.
(40) Brookes, N. J.; Graham, D. C.; Christian, G.; Stranger, R.; Yates, B. F. *J. Comput. Chem.* **2009**, *30*, 2146−2156.
(41) Cui, Q.; Musaev, D. G.; Svensson, M.; Sieber, S.; Morokuma, K. *J. Am. Chem. Soc.* **1995**, *117*, 12366−12367.